PHYSICAL REVIEW A **86**, 043423 (2012)

Femtosecond-pulse-train ionization of Rydberg wave packets

S. I. Simonsen,* S. A. Sørngård,† M. Førre, and J. P. Hansen
Department of Physics and Technology, University of Bergen, N-5007 Bergen, Norway
(Received 25 June 2012; revised manuscript received 9 August 2012; published 19 October 2012)

We calculate, based on first-order perturbation theory, the total and differential ionization probabilities from a dynamic periodic Rydberg wave packet of a given n-shell exposed to a train of femtosecond laser pulses. The total probability is shown to depend crucially on the laser repetition rate: For certain frequencies the ionization probability vanishes, while for others it becomes very large. The origin of this effect is the strong dependence of the ionization probability on the Stark quantum number. Correspondingly, the angular electronic distribution also changes significantly with the increasing number of pulses for certain repetition rates.

DOI: 10.1103/PhysRevA.86.043423 PACS number(s): 32.80.Fb, 32.80.Ee, 32.80.Rm, 32.60.+i

I. INTRODUCTION

Exposure of atoms to short attosecond pulse trains phase-locked onto femtosecond pulses has recently given direct insight into electronic ground-state dynamics as the atom is perturbed by the femtosecond laser field [1,2]. The key ingredient which allows mapping between spectra of electron momenta and initial state dynamics is the very short and phase-locked attosecond burst as compared to the much slower original femtosecond laser pulse. A related experiment can be suggested based on highly excited atoms and on a much slower time scale: a train of femtosecond laser pulses firing on top of a microwave field which drives a Rydberg wave packet. The ionizing femtosecond pulse could in this case serve as a sensitive camera which could reconstruct the image of exotic electronic states on the border between classical physics and quantum dynamics.

The ionization of Rydberg atoms by femtosecond laser fields has been studied both experimentally and theoretically. For example, on the experimental side electron dynamics following two controlled time-delayed pulses has shown distinct electron emission characteristics [3,4]. On the theory side strong effects of counterpropagating pulses on Rydberg atom ionization probability have been predicted [5]. Recently, the ionization of low-lying circular Rydberg states exposed to circularly polarized laser fields was investigated both by solving the Schrödinger equation and by using the classical trajectory Monte Carlo (CTMC) method [6]. CTMC calculations have also been used extensively in exploring Rydberg atoms with very high principal quantum numbers, lately in the study of localized Bohr-like wave packets [7–9].

Several studies have investigated the dynamics of inter-n Rydberg wave packets in static electric fields through their ionization by half-cycle electric field pulses that ionize the wave packet during its motion [10,11]. More recently, the response of dynamic Rydberg wave packets created by a picosecond laser pulse from the Li($3d$) state in the presence of an inter-n mixing microwave field has been reported [12]. A strong modification of the selective field ionization (SFI) signal depending on the wave packet creation time with respect to the phase of the microwave field was detected.

Previous experimental works have considered wave packet dynamics and ionization where the Rydberg atom is exposed to strong n-mixing fields [10]. Here we consider theoretically the ionization signature of a related but different wave packet which can be created within a single n level when the atom is exposed to much weaker electric fields, below the Inglis-Teller limit, $1/3n^5$ (a.u.) [13]. The intra n-shell (angular) wave packet of hydrogen is driven by a microwave time-dependent electric field and exposed to a train of ionizing femtosecond laser pulses. The microwave field in our setup drives a wave packet of a given n-shell periodically between a maximum polarized (linear) Stark state and a circular state [14,15]. The ionization probability and electron emission characteristics are calculated as function of the number of laser pulses and the time separation between the pulses. The single-pulse ionization probability is found to be orders of magnitude larger for high Stark quantum numbers compared to the lower ones, and the angular emission spectra are shown to be detailed functions of the number of times the Rydberg wave packet is hit in highly polarized vs unpolarized states. Once the highly polarized states are hit they dominate the angular emission spectra completely.

In the following section we outline the theory and in the subsequent section results are discussed. Atomic units, where m_e, $\hbar$, and e are scaled to unity, are used throughout unless stated otherwise.

II. THEORY

Our starting point is a Rydberg wave packet driven in a Stark setup [16–18] by a resonant rotating microwave field,

$$\mathbf{E}_\mu(t) = \epsilon_0 \cos\omega_\mu t\,\hat{x} - \epsilon_0 \sin\omega_\mu t\,\hat{y} - \epsilon_z \hat{z}, \qquad (1)$$

repeatedly between the circular ($|km\rangle = |0\ m_{\max}\rangle$) and the linear ($|km\rangle = |k_{\max}\ 0\rangle$) state in the Stark manifold, as shown in color in Fig. 2. k denotes the Stark quantum number. The field strength of the oscillating xy components is $\epsilon_0 = 10^{-8}$a.u., whereas the constant z component $\epsilon_z = 10^{-7}$a.u. induces a Stark energy splitting $\Delta E_z = 3/2n\epsilon_z = \omega_\mu = 2.4 \times 10^{-6}$a.u. When calculating matrix elements of the dipole operator within a principal n-shell the operator replacement $\hat{r} \to 3n/2\hat{a}$ [19] may be performed, where $\hat{a}$ is the operator for the Runge-Lenz vector. Since this operator behaves identically to a spin operator with each Stark state being eigenstates of $\hat{a}^2$ and $\hat{a}_z$, the selection rule $|\Delta k| = 1$ follows directly, as a parallel to

*sigrid.simonsen@ift.uib.no
†stian.sorngard@ift.uib.no

the well-known selection rule $|\Delta m| = 1$ in the spherical basis. Due to the clockwise rotation of the resonant microwave field, one-photon absorption and emission solely allow transitions satisfying the selection rules $\Delta m = \pm 1$ and $\Delta k = \mp 1$. The wave packet will make one round trip along the Stark ladder in about ten revolutions of the microwave field.

We consider the situation where the wave packet slowly evolving in the microwave field is hit by a series of short femtosecond laser pulses. We assume that only a small fraction of the wave packet is launched to the continuum at each pulse; thus from first-order time-dependent perturbation theory the transition amplitude from the jth pulse in the pulse train reads

$$a_{qlm}^{(j)} = -i \int_{t_j}^{t_j+T} \langle \psi_{qlm} | V(t) | \Psi_b(t_j) \rangle e^{i(E_q - E_b)t} dt, \qquad (2)$$

where q is the momentum of the ionized electron and T is the pulse duration of each pulse. The present Stark shift ΔE_z is of the order of 10^{-6}a.u., which is negligible compared to the binding energy of the $n = 16$ level without the Stark shift ($I_p \approx 0.002$ a.u.) when probing with an 800-nm pulse.

The bound electron wave function $\Psi_b(t)$ in Eq. (2) can be described as

$$|\Psi_b(t)\rangle = \sum_{k,m} c_{km}(t) |\psi_{nkm}\rangle, \qquad (3)$$

where $|\psi_{nkm}\rangle$ denotes the Stark states. These can in turn be expanded in the spherical basis states $|\psi_{nlm}\rangle$ [20],

$$|\psi_{nkm}\rangle = \sum_l (-1)^l \left\langle \frac{n-1}{2}, \frac{m-k}{2}, \frac{n-1}{2}, \frac{m+k}{2} \middle| lm \right\rangle |\psi_{nlm}\rangle. \qquad (4)$$

The amplitudes are Clebsch-Gordan coefficients, and we refer to them as b_{klm}. This gives the following expression for the bound state at time t:

$$|\Psi_b(t)\rangle = \sum_{k,m} \sum_l c_{km}(t)\, b_{klm}\, |\psi_{nlm}\rangle. \qquad (5)$$

The coupling $V(t) = \mathbf{E}(t) \cdot \mathbf{r}$ in Eq. (2) is the laser-matter interaction within the dipole approximation when represented in the length gauge. Due to the short duration of the pulse ($\sim 10^2$ a.u.) compared to the time of evolution of the bound wave packet in the microwave field ($\sim 10^6$ a.u.), we neglect the effect of the microwave field during the action of the femtosecond probe pulse. In addition, due to the finite spectral width of the short ionizing pulse, excited (bound) states are populated throughout the interaction with the laser field, but the population in these states is nevertheless so small that it does not influence the subsequent ionization dynamics.

After interaction with a pulse train of N pulses separated by a time Δt, the continuum part of the total wave function of the system can be written as

$$|\Psi_c\rangle = \sum_{q,l,m} \sum_{j=1}^{N} a_{qlm}^{(j)} |\psi_{qlm}\rangle e^{-iE_q(N-j)\Delta t}, \qquad (6)$$

giving the following amplitudes for the final continuum states,

$$\alpha_{qlm} = \sum_{j=1}^{N} a_{qlm}^{(j)} e^{-iE_q(N-j)\Delta t}. \qquad (7)$$

Moreover, the continuum wave function is expanded in Coulomb partial waves $|\psi_{qlm}\rangle$, which conform to incoming boundary conditions,

$$\langle r | \psi_{qlm} \rangle = i^l e^{-i\sigma_l} Y_{lm}(\hat{r}) Y_{lm}^*(\hat{q}) R_{ql}(r), \qquad (8)$$

where $\sigma_l = \arg \Gamma(l + 1 - i/q)$ is the Coulomb phase shift of the lth partial wave. The radial part, when normalized in momentum space, reads [21]

$$R_{ql}(r) = \sqrt{\frac{2}{\pi}} \frac{e^{\pi/2q} |\Gamma(l + 1 - i/q)|}{(2l+1)!} (2r)^l q^{l+1} e^{-iqr} \times {}_1F_1(l + 1 + i/q, 2l + 2, 2iqr). \qquad (9)$$

In the computations we have utilized the Coulomb wave implementation provided by the GNU Scientific Library (GSL) [22]. It should also be noted that the corresponding energy-normalized wave function is conveniently obtained through the scaling relation $R_{E_q l}(r) = q^{-1/2} R_{ql}(r)$.

To model the laser pulse we use a plane wave in the z direction modulated by a sine-square carrier envelope. The time-dependent electric field is derived from the vector potential

$$\mathbf{A}(t) = A_0 \sin^2 \left[\frac{\pi(t - t_j)}{T} \right] \sin[\omega(t - t_j)] \hat{z}, \qquad (10)$$

through the relation $\mathbf{E}(t) = -\partial_t \mathbf{A}(t)$, where the central frequency ω of the plane wave corresponds to $\lambda = 800$ nm. The electric field strength is $E_0 = 2.0 \times 10^{-5}$ a.u. ($I_{\text{peak}} = 1.4 \times 10^7$ W cm^{-2}), and the duration of the pulse is given by $T = 2\pi N_{\text{oc}}/\omega$. In our calculations we have set the number of optical cycles $N_{\text{oc}} = 4$, which corresponds to a pulse duration of $T = 441$a.u. $= 11$fs.

With the amplitudes of the continuum wave packet at hand the differential probability is readlily obtained:

$$\frac{dP}{dq d\Omega} = \left| \sum_{l,m} \alpha_{qlm} \right|^2. \qquad (11)$$

Integrating out the momentum gives the angular resolved ionization probability,

$$\frac{dP}{d\Omega}(\theta, \phi) = \int \left| \sum_{l,m} \alpha_{qlm} \right|^2 q^2 dq, \qquad (12)$$

and alternatively, by performing the angular integral we obtain the energy spectrum,

$$\frac{dP}{dE_q} = \sum_{l,m} |\alpha_{qlm}|^2, \qquad (13)$$

with $E_q = q^2/2$. For the sake of consistency, notice that in the latter formula the amplitudes α_{qlm} are energy normalized. Finally, the ionization probability is given by

$$P = \int \sum_{l,m} |\alpha_{qlm}|^2 q^2 dq. \qquad (14)$$

In order to check the validity of the adopted first-order time-dependent perturbation theory approach, we compare in Fig. 1 the ionization probability so obtained with the exact

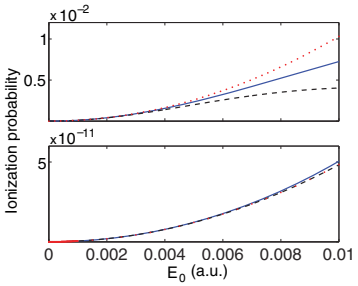

FIG. 1. (Color online) Ionization probability for a single pulse calculated using perturbation theory (red, dotted lines) and exact solution (blue, full lines) as a function of electric field strength E_0. A four-cycle laser pulse of the form given in Eq. (10) was used in the calculations. The initial states are $|nlm\rangle = |16\ 0\ 0\rangle$ (upper panel) and $|nlm\rangle = |16\ 15\ 15\rangle$ (lower panel). Also shown are the partial contributions of the $l = 1$ channel and the $l = 16$ channel (black, dashed lines) in the upper and lower panels, respectively. In the lower panel the three lines coincide.

one. The figure depicts the ionization probability for a single four-cycle pulse as a function of the electric field strength E_0 of the applied laser field. The upper and lower panels show the results for the initial states $|nlm\rangle = |16\ 0\ 0\rangle$ and $|nlm\rangle = |16\ 15\ 15\rangle$, respectively. Figure 1 also shows the partial contribution of the $l = 1$ channel (upper panel) and the $l = 16$ channel (lower panel) to the total ionization yield (red, dashed line), as obtained from the full calculation. The full calculations are performed using a spectral method where the eigenstates are expanded in either a Fourier series (in the case of the circular initial state) or a B-spline basis set (in the case of the $16s$ initial state), imposing a zero boundary condition at the edge of the radial box of some finite size $R_{\max}$. In the calculations $R_{\max}$ is varied in the interval 2400–5000 a.u. and the velocity gauge is assumed. Furthermore, angular momenta up to $l = 19$ are included in the basis set. As such, the results are checked for convergence with respect to both the number of angular momenta included and the size of the radial box. Figure 1 clearly indicates that the first-order time-dependent perturbation theory approach is valid up to electric field strengths of the order of 0.001 a.u., ensuring that the laser field applied in the present work ($E_0 = 2.0 \times 10^{-5}$a.u.) is well within the perturbative regime.

The ionization probabilities of Rydberg states are extremely small, and it is therefore important that the continuum is well represented, especially when calculating the angular-resolved ionization probability. Thus, we have conducted test calculations using different densities of states in the continuum discretization to make sure all quantities are converged.

Note finally that the widely used alternative perturbation theory based on Volkov waves completely fails in general when considering initial Rydberg states: Orders of magnitude discrepancies with exact calculations are obtained when replacing our final states with Volkov waves. The origin of the failure can be traced to the sensitivity of the initial state to

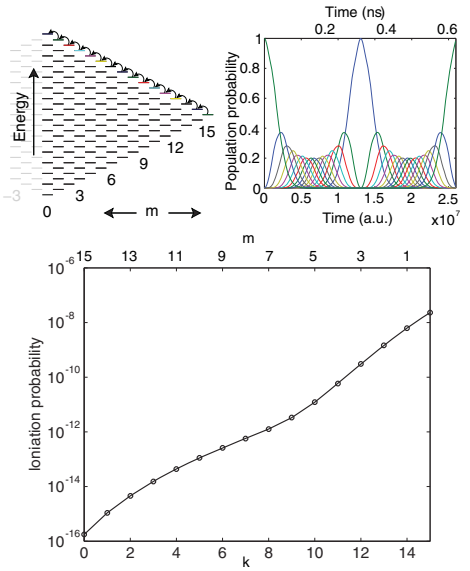

FIG. 2. (Color online) Upper left panel: Stark states $|km\rangle$ of the $n = 16$ level due to the constant electric field ϵ_z. Only the states with $m \geqslant 0$ are shown. The states populated by the rotating microwave field in the xy plane are shown in color and with arrows. Upper right panel: The population of the (colored) Stark states as a function of time for one round trip in the Stark setup, corresponding to time $\tau = 2.61 \times 10^7$ a.u. The initial state is the circular Stark state. After half the cycle τ the most polarized state is fully populated while the circular state is depleted. At the end of the round trip the circular state is totally revived. Lower panel: The ionization probability of the relevant Stark $|km\rangle$ states when fully populated. Field parameters are given in the text.

electric fields. Other methods, like the sudden perturbation approximation [5,23], have been used on Rydberg atoms exposed to ultrashort laser pulses, but are not invoked here due to the good agreement between first-order perturbation theory and exact calculations.

III. RESULTS

Before discussing the main findings it may be instructive to have a closer look at Fig. 2. The upper right panel shows the population probability for the states involved in one round trip in the Stark manifold (depicted in the left panel of the same figure). The period of this round trip is $\tau = 2.61 \times 10^7$ a.u. (0.63 ns), which again corresponds to about 10 times the period of the rotating microwave field in the xy plane. The wave function of the bound electron undergoes intrashell transitions, according to the selection rules $\Delta m = \pm 1$ and $\Delta k = \mp 1$, implying that only the "outermost" Stark states, i.e., the states

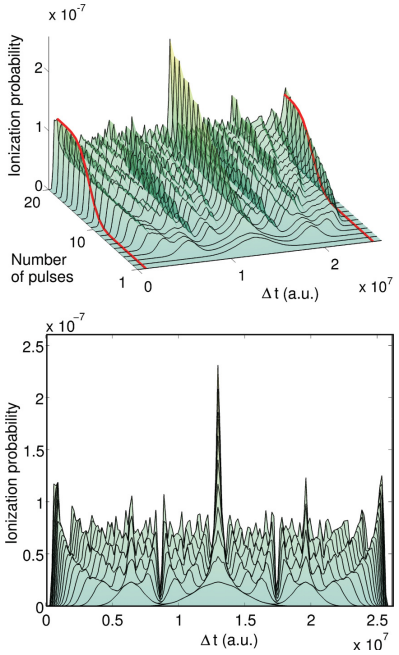

FIG. 3. (Color online) Ionization probability [cf. Eq. (14)] as a function of N succeeding pulses and time delay Δt. The initial state is the circular Stark state, $|nkm\rangle = |16\ 0\ 15\rangle$, and the maximum time separation $\tau = 2.61 \times 10^7$ a.u. corresponds to the revival time of the initial state in the microwave field. The lower panel shows the front view of the landscape plotted above. The minimum occurs at $\Delta t = 0$ and τ, but at time steps corresponding to $\tau/3$ and $2\tau/3$, there is only a small increase in the probability. The maximum is reached when pulses are separated by $\tau/2$, causing every second pulse to hit the most polarized Stark state. The thick red curves indicate the pulse sequences with $\Delta t = 9 \times 10^5$ a.u. and $\Delta t = 2.52 \times 10^5$ a.u. especially mentioned in Sec. III. Field parameters are given in the text.

with $m = n - k - 1$, are populated (cf. the upper left panel in Fig. 2).

The ionization probability of the Stark states in question, when fully populated, greatly varies in magnitude with increasing k, as the lower panel in Fig. 2 displays. The difference in ionization probability for the circular and linear states is of eight orders of magnitude, and this is related to the electron's ability to interact with the nucleus. The linear-most states are the states containing components of low angular momentum, which means that they are more likely to come close to the nucleus and hence are more likely to be slung out of the atom. The leap in the ionization probability is important for the understanding of what happens when the Stark manifold is hit by the pulse train and is referred to later in the discussion.

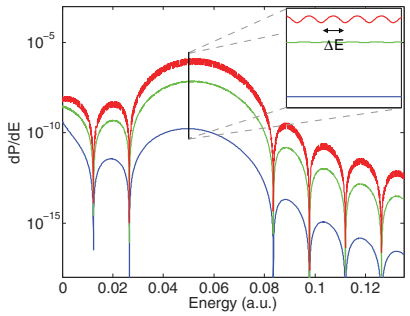

FIG. 4. (Color online) Energy distribution of the continuum wave packet for a series of pulses, $N = 3$ (lower, blue line), 4 (middle, green line), and 5 (upper, red line). The time separation between the pulses is $\Delta t = 3 \times 10^6$ a.u. Succeeding pulses hitting states with ionization probability differing only a few orders in magnitude cause interference in the continuum wave packet as observed between the fourth and the fifth pulse (upper line). The inset shows a closeup of the distributions on the interval $(0.05, 0.05 + 10^{-5})$ a.u. The period of the oscillations clearly matches the time delay between the pulses, i.e., $\Delta E = 2\pi/\Delta t \simeq 2.1 \times 10^{-6}$a.u. Field parameters are given in the text.

Figure 3 shows the total ionization probability [cf. Eq. (14)] of the Rydberg atom as a function of the number of femtosecond laser pulse shots N and the time delay Δt between the pulses. In each specific pulse train the pulses are equally separated in time. The initial state prior to the pulse train is the circular state $|nkm\rangle = |16\ 0\ 15\rangle$. In between the pulses in the pulse train the wave function of the bound electron undergoes intrashell transitions according to the scheme in Fig. 2, changing the state subject to ionization at each laser shot. The different pulse rates seem to yield approximately the same total ionization probability after the train of 20 pulses has passed, with the exception of six time separations Δt, for which the ionization probability is either strongly increased or totally suppressed. For $\Delta t \simeq 0$ and $\Delta t = \tau$ the pulse train hits the circular state at every impact, and thus the ionization probability remains at an absolute minimum at all times. The maximum is reached when $\Delta t = \tau/2$, causing every second pulse to hit the linear state, hence giving maximum contribution to the probability. A closer examination of the two valleys at $\Delta t = 8.7 \times 10^6$a.u. $= \tau/3$ and $\Delta t = 1.74 \times 10^7$a.u. $= 2\tau/3$ reveals that the ionization probability has a very small increase with N. This suggests, in light of the previous discussion, that for time separations corresponding to $\tau/3$ and $2\tau/3$ the laser pulses hit the wave packet only in states nearby, but not sufficiently close to, the linear state. It is interesting to notice that these are the only pulse rates, except for $\Delta t = 0$ and $\Delta t = \tau$, that seem to give such a behavior.

In addition, the total ionization probability depends on how many succeeding pulses are hitting the atom. As seen in the upper panel of Fig. 3 some time separations, like $\Delta t = 9 \times 10^5$ a.u. and $\Delta t = 2.52 \times 10^7$ a.u., yield a very slow increase

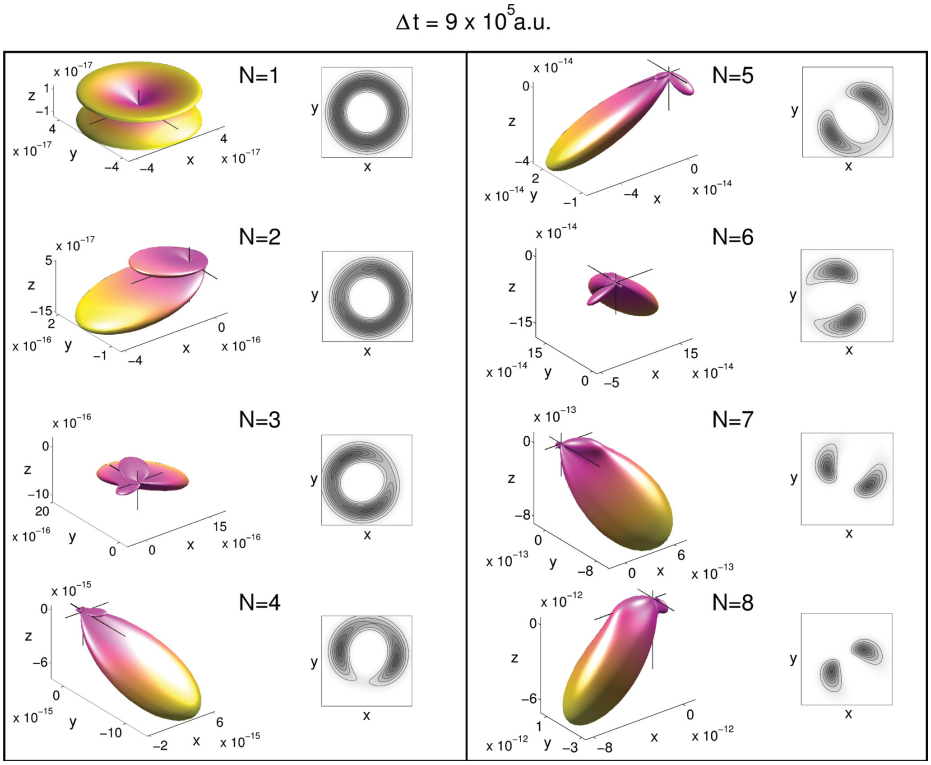

FIG. 5. (Color online) To the left in both panels are plotted the angular-resolved ionization probability $dP/d\Omega$ [c.f. Eq. (12)] for a series of N succeeding pulses with time separation $\Delta t = 9 \times 10^5$ a.u. To guide the eye we have included an auxiliary set of axes indicating the position of the origin. We observe that the distribution in the continuum rotates clockwise about the z axis with a period that is comparable to the period of the rotating microwave field. The right figures show cuts in the xy plane for the corresponding electron density distribution of the bound wave function from which the ionization happens. The initial state for the pulse train is the circular Stark state. Field parameters are given in the text.

in the ionization probability for the first 10 pulses, but a strong increase from 10 to 20 pulses. These two pulse sequences are shown as red (thick) curves in Fig. 3.

The energy spectrum, obtained by Eq. (13), of the total continuum wave packet after three, four, and five pulses are shown in Fig. 4, when the pulses are separated by $\Delta t = 3 \times 10^6$ a.u. As expected the distribution is dominated by the large one-photon resonance centered around the laser frequency $\omega = 0.057$ a.u. (800 nm). The side peaks in the spectrum can be attributed to the side bands of the sine-squared pulse envelope. More interestingly, one makes out some small oscillations superimposed on the energy spectrum of the fifth pulse, as can be seen in the inset of Fig. 4, where the energy distribution is plotted on a finer grid to obtain better resolution. These oscillations are caused by the interference between the wave packet launched to the continuum by the fifth pulse and the wave packet that is already there. We see that the period of the oscillations in question indeed corresponds to the time delay between the pulses, i.e., $\Delta E = 2\pi/\Delta t \simeq 2.1 \times 10^{-6}$ a.u. The interference effect is most pronounced when two succeeding wave packets are of comparable amplitudes, which is the case for the fourth and the fifth pulse (cf. upper panel of Fig. 3). One also notices that the relative height of the slow-electron peak close to the origin as compared to the one-photon resonance peak changes with number of pulses. These two peaks are the results of two different ionization processes. The first is the response to the electron cloud being pulled away from the nucleus, resulting in low-energy electrons being released from the core potential. The latter, dominating as the bound state gradually approaches the linear state, comes from the electron being "kicked out" when interacting with the nucleus, creating ionized electrons of higher energy.

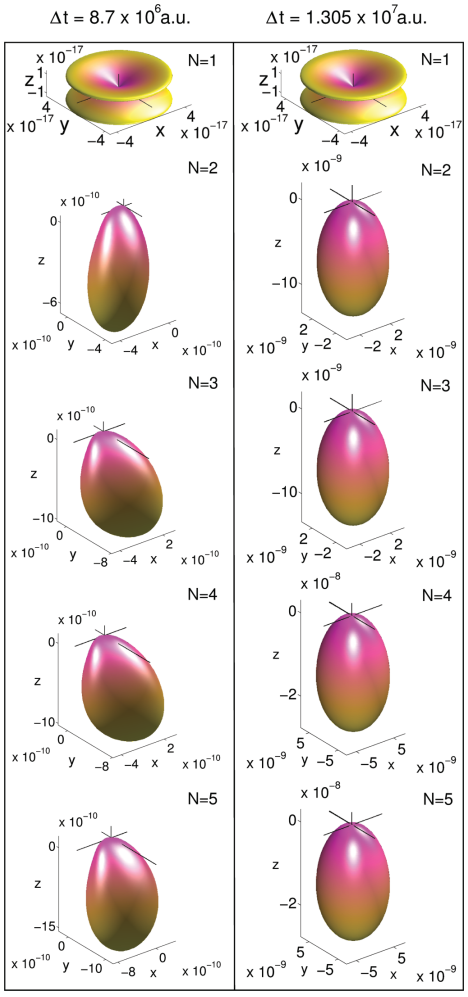

FIG. 6. (Color online) The figure shows the angular-resolved ionization probability $dP/d\Omega$ [cf. Eq. (12)] for five succeeding pulses. Starting in the circular Stark state the left column and the right column show the distribution when the time between the pulses is $\Delta t = 8.7 \times 10^6$ a.u and $\Delta t = 1.305 \times 10^7$a.u., respectively. To guide the eye we have included an auxiliary set of axes indicating the position of the origin. Field parameters are given in the text.

In Figs. 5 and 6 we consider the angular distribution of the ionized electron. In these figures we have plotted the angular-resolved ionization probability [cf. Eq. (12)] for a series of pulses of three different Δt. The first plot in all the three series corresponds to the initial state being the circular state. We see that the continuum wave packet for this state is symmetric about the z axis, as expected. To the left in both columns of Fig. 5 the evolution of the continuum from eight succeeding pulses with $\Delta t = 9 \times 10^5$ a.u. is shown. This is the time step causing the first peak in the plot of the total ionization probability (lower panel of Fig 3). The pulse repetition rate is so high that the bound wave packets do not have time to climb more than half the Stark ladder, and consequently the total ionization probability remains relatively low for the first eight pulses. It is interesting to observe that the main lobe of the angular distribution in this case seems to rotate clockwise about the z axis, and by careful examination of its period of rotation, it can be identified to match the period of the microwave field. This shows that femtosecond pulses firing on top of time-dependent radio frequency or microwave fields will, together with angular-resolved detection methods, serve as a direct camera of wave packet dynamics. To the right in the figure we have plotted a cut of the electron density distribution in the xy plane of the bound wave packet from which the ionization happens for each pulse N. The electron density rotates clockwise with the period of the rotating field, causing the rotation in the continuum distribution. Interestingly, it seems that the main lobe of the continuum distribution is turned a bit to the left from the least dense part of the bound wave packet for all pulses.

Starting with the right column of Fig. 6, we have plotted the angular distributions pertaining to the main ridge in Fig. 3. This is the special case in which the pulse train is tuned to strike the bound wave packet at times where it alternates between being at its most polarized and unpolarized, i.e., $\Delta t = \tau/2$. We observe that from the second pulse the distribution remains, for all practical means, unchanged throughout the pulse train. Taking into account that the first pulse hits the circular state, the next one hitting the linear state will completely overshadow the ionization from the first strike. The reason is evident when looking at Fig. 2, the linear Stark state, as compared to the circular Stark state, is by far more prone to be ionized.

Finally, we turn our attention to the left column of Fig. 6. The angular distributions in these plots correspond to the time step $\Delta t = \tau/3$ (cf. the first valley in Fig. 3). The difference in the repetition rate, as compared to the one in the right column, entails the femtosecond pulse hitting several states close to the linear one, and hence it introduces an asymmetry in the distributions. Comparing the two columns we see that though the distribution remains mostly along the negative z direction with increasing N for both cases, the ionization probability for $\Delta t = \tau/2$ is about an order of magnitude larger than that for $\Delta t = \tau/3$. It should also be mentioned that for increasing numbers of pulses, the ionization probability for $\Delta t = \tau/3$ will remain of the same order of magnitude as seen in Fig. 6, while for $\Delta t = \tau/2$ it will roughly be doubled for every other pulse.

IV. CONCLUSION

In this work we have studied features of single-electron ionization of a *dynamic* intra n-shell wave packet as compared to ionization from stationary states. Since the ionization probabilities of the stationary states vary largely with the

degree of polarization (Stark quantum number), a strong sensitivity of the ionization probability to the repetition rate of the ionizing laser pulses occurs. In the most extreme cases the total ionization probability after a number of N pulses varies from almost zero to $N/2$ times the ionization probability of the maximum polarized Stark state. Moreover, the angular differential ionization probabilities are shown to be intimately related to the number of times the pulse train strikes the bound wave packet. The near-circular wave packets exhibit rotation in the xy plane due to the rotating microwave field, which is reflected in the continuum distribution. On the other hand, when the near-linear states are probed, the rotation in the continuum is completely overshadowed by the symmetric distribution of the highly polarized states in the z direction. Nevertheless, these findings suggest that more complex periodic dynamics of a Rydberg atom, for example, oscillations from classical to nonclassical states, may be monitored by weak ionizing femtosecond pulse trains.

ACKNOWLEDGMENTS

This project was supported by the Research Council of Norway (RCN) and the Bergen Research Foundation (Norway).

[1] J. Mauritsson, P. Johnsson, E. Mansten, M. Swoboda, T. Ruchon, A. L'Huillier, and K. J. Schafer, Phys. Rev. Lett. **100**, 073003 (2008).

[2] P. Johnsson, J. Mauritsson, T. Remetter, A. L'Huillier, and K. J. Schafer, Phys. Rev. Lett. **99**, 233001 (2007).

[3] M. L. Bajema, R. R. Jones, and T. F. Gallagher, Phys. Rev. A **70**, 062722 (2004).

[4] J. G. Story and H. N. Ereifej, Phys. Rev. Lett. **86**, 612 (2001).

[5] A. V. Lugovskoy and I. Bray, Phys. Rev. A **73**, 063401 (2006).

[6] S. Askeland, S. A. Sørngård, I. Pilskog, R. Nepstad, and M. Førre, Phys. Rev. A **84**, 033423 (2011).

[7] J. J. Mestayer, W. Zhao, J. C. Lancaster, F. B. Dunning, C. O. Reinhold, S. Yoshida, and J. Burgdörfer, Phys. Rev. Lett. **99**, 183003 (2007).

[8] J. J. Mestayer, B. Wyker, J. C. Lancaster, F. B. Dunning, C. O. Reinhold, S. Yoshida, and J. Burgdörfer, Phys. Rev. Lett. **100**, 243004 (2008).

[9] B. Wyker, S. Ye, F. B. Dunning, S. Yoshida, C. O. Reinhold, and J. Burgdörfer, Phys. Rev. Lett. **108**, 043001 (2012).

[10] C. Raman, T. C. Weinacht, and P. H. Bucksbaum, Phys. Rev. A **55**, R3995 (1997) .

[11] M. B. Campbell, T. J. Bensky, and R. R. Jones, Phys. Rev. A **59**, R4117 (1999).

[12] K. R. Overstreet, R. R. Jones, and T. F. Gallagher, Phys. Rev. A **85**, 055401 (2012).

[13] D. R. Inglis and E. Teller, Astrophys. J. **90**, 439 (1939).

[14] M. Førre, H. M. Nilsen, and J. P. Hansen, Phys. Rev. A **65**, 053409 (2002).

[15] L. Sælen, S. I. Simonsen, and J. P. Hansen, Phys. Rev. A **83**, 015401 (2011).

[16] R. G. Hulet and D. Kleppner, Phys. Rev. Lett. **51**, 1430 (1983).

[17] J. C. Day, T. Ehrenreich, S. B. Hansen, E. Horsdal-Pedersen, K. S. Mogensen, and K. Taulbjerg, Phys. Rev. Lett. **72**, 1612 (1994).

[18] R. Lutwak, J. Holley, P. P. Chang, S. Paine, D. Kleppner, and T. Ducas, Phys. Rev. A **56**, 1443 (1997).

[19] W. Pauli, Z. Phys. **36**, 336 (1926).

[20] T. F. Gallagher, *Rydberg Atoms* (Cambridge University Press, Cambridge, UK, 1994).

[21] H. A. Bethe and E. E. Salpeter, *Quantum mechanics of One- and Two-Electron Atoms* (Springer-Verlag, Berlin, 1957).

[22] The GNU Scientific Library, www.gnu.org/software/gsl.

[23] A. V. Lugovskoy and I. Bray, Phys. Rev. A **72**, 063402 (2005).